Journal of Sound and Vibration (1999) **219**(5), 859–879
Article No. jsvi.1998.1905, available online at http://www.idealibrary.com on IDEAL

MODELLING THE INFLUENCE OF ACOUSTIC LINER NON-UNIFORMITIES ON DUCT MODES

B. REGAN AND J. EATON

Aerospace Research Unit, National University of Ireland, Galway, Ireland

(*Received* 30 *January* 1998, *and in final form* 10 *August* 1998)

In most turbofan engine intakes, the acoustically lined region consists of several liner segments which are separated by longitudinal hard-walled intercostal strips or splices. Measurements indicate that the duct modal spectrum can be considerably altered by such circumferential variations in acoustic properties, with energy being transferred from an incident mode to several others. To investigate and quantify this phenomenon, a three-dimensional, frequency domain finite element method has been developed. The computational domain represents a length of infinite, hard-walled duct of circular cross-section fitted with a region of longitudinally spliced liner. A modal coupling scheme is used, in which complex modal input amplitudes are specified across a section at one end of the computational duct domain and the amplitudes and phases of the transmitted modes are captured at the other end. In addition, to model the convective effect of flow in the duct, a uniform, unidirectional flow field is treated. The method is verified by comparing predictions with analytical solutions and is then used to analyze a liner with splices. It is demonstrated that incident modes are significantly affected by the circumferential variations in impedance and as such, the influence of liner splices on the transmitted acoustic field ought to be further investigated.

1. INTRODUCTION

For convenience and cost of manufacturing, the acoustic liner installed in turbofan engines consists of several segments, divided by longitudinal strips or splices which are essentially hard-walled (see Figure 1). It has long been suspected that such circumferential discontinuities of impedance might have a significant effect on the radiated sound field, by causing incident modes to be scattered so that their energy is transmitted into different modes. Unless this modulation of the transmitted acoustic field is accounted for at the design stage of the turbofan intake liner, the splices are likely to have an adverse affect on the liner noise attenuation performance. Experimental investigations have indeed verified this to be the case. In-flight measurements [1] of the circumferential modal spectra of hte Rolls-Royce Tay 650 engine installed in the Fokker 100 aeroplane indicated that the sound field radiating from the inlet was substantially affected by the presence of splices. Further flight tests of the same engine fitted with a single piece liner demonstrated a significantly attenuated noise field compared to the same engine with a

0022–460X/99/050859 + 21 $30.00/0

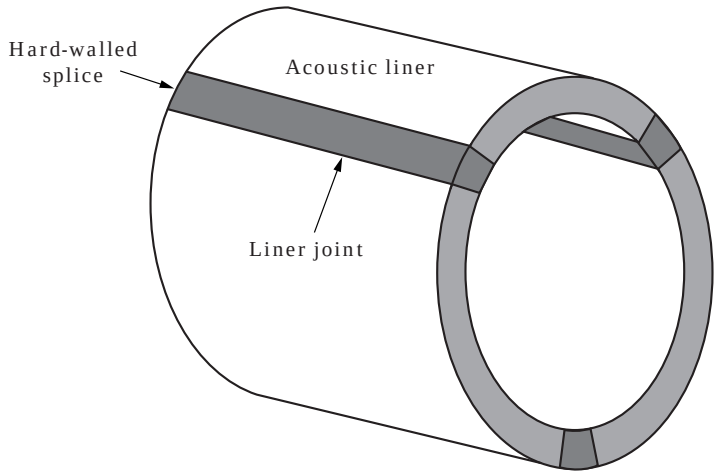

Figure 1. Sketch of liner barrel with intercostal strips (longitudinal splices).

three-splice liner. Ohter experimental studies [2, 3] have since corroborated these findings.

While single piece liner barrels are attractive as a means of improving attenuation performance, in general this is not economically feasible because of manufacturing and design constraints. It is therefore useful to develop analytical tools to study and quantify the influence of intercostal strips. Such tools could then be used for design purposes to predict the effect of the number of strips and their width, layout and shape on a selection of incident modes, over a range of frequencies and Mach numbers.

In this work, an existing three-dimensional finite element method is developed to model the propagation of cross-sectional modes over a lined region of an infinite duct in the presence of a uniform airflow (see Figure 2). The effect of the liner, which is assumed to be locally reacting, is represented by specifying an impedance on the inner duct wall over the lined region. The intercostal strips are assumed to be acoustically hard-walled, which is equivalent to an infinite impedance condition. Complex incident modal amplitudes are injected at an input

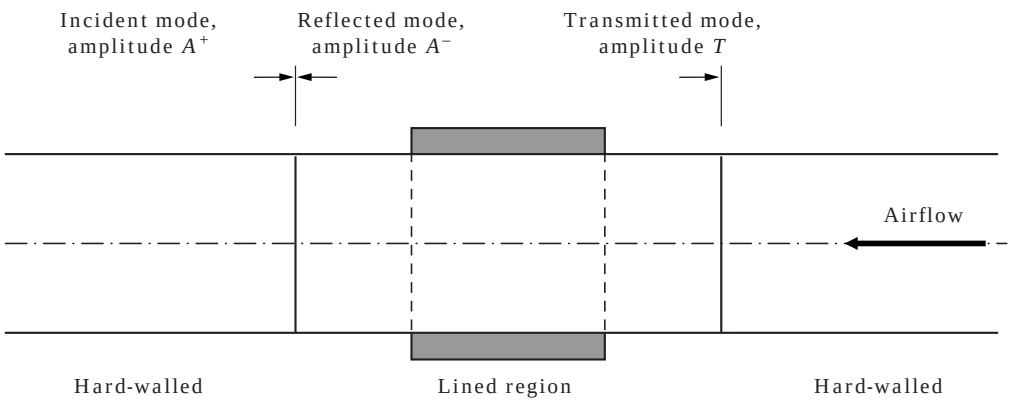

Figure 2. Incident, reflected and transmitted modes in numerical duct model.

cross-section (the modal input plane) and the complex amplitudes of the reflected an transmitted modes emerge as part of the solution. The amplitudes of the modes that are excited by the scattering can therefore be determined from the transmitted modal spectrum.

The computational cost of three-dimensional acoustic problems rapidly becomes demanding as frequency is increased, since, when using the finite element method, a minimum of five quadratic elements per wavelength is typically required in each co-ordinate direction to accurately resolve the acoustic field [4, 5]. To enable the solution of duct configurations at reasonable reduced frequencies by using modest computing facilities, a preconditioned iterative solver is employed. Drawing on past experience [4–6], an ILU(0) preconditioner is used in conjunction with the biconjugate gradient iteration algorithm.

This paper is laid out as follows. The mathematical model, consisting of governing equations, boundary conditions and treatment of the modal interface is described. We then outline the formulation of the three-dimensional finite element representation of the model and the iterative solution procedure. The numerical model is then verified by comparing its predictions with analytical solutions for two basic test case configurations. Further verification is achieved by using a third configuration; an axisymmetric, axially varying liner, where predictions are compared with semi-analytical solutions. Finally, the application of the prediction method for realistic spliced arrangements is demonstrated by analyzing the behaviour of a lined region of duct with two splices.

2. MATHEMATICAL MODEL

2.1. GOVERNING EQUATIONS

It is assumed that the fluid medium is inviscid and non-heat conducting with constant specific heats, and that all acoustic processes are isentropic. Furthermore, it is assumed that the airflow is uniform and unidirectional, with the flow being aligned with the duct axis. Under these assumptions, the convected wave equation governs acoustic propagation,

$$\nabla^2 p - \frac{1}{c^2}\frac{\mathrm{D}^2 p}{\mathrm{D}t^2} = 0, \tag{1}$$

where the total derivative is defined as:

$$\mathrm{D}/\mathrm{D}t = \partial/\partial t + M\partial/\partial x \tag{2}$$

when the flow velocity is aligned with the x direction (a list of nomenclature is given in the Appendix). The frequency domain version of the convective wave equation is derived by assuming that the acoustic disturbances vary harmonically with time dependence $\mathrm{e}^{\mathrm{i}\omega t}$. The resulting acoustic fluctuations then take the form

$$p(x, y, z, t) \rightarrow p(x, y, z)\,\mathrm{e}^{\mathrm{i}\omega t} \tag{3}$$

and the convected wave equation reduces to

$$\nabla^2 p - \frac{1}{c^2}\left(\mathrm{i}\omega + M\frac{\partial}{\partial x}\right)^2 p = 0, \tag{4}$$

which, upon expanding, can be expressed as

$$(1 - M^2)\frac{\partial^2 p}{\partial x^2} - 2\mathrm{i}kM\frac{\partial p}{\partial x} + \frac{\partial^2 p}{\partial y^2} + \frac{\partial^2 p}{\partial z^2} + k^2 p = 0. \tag{5}$$

2.2. BOUNDARY CONDITIONS

The intercostal strips on the liner surface can essentially be considered as hard-walled. An acoustically hard surface is one which is totally reflective, and on which the normal component of acoustic velocity is zero, so that

$$\mathbf{v} \cdot \mathbf{n} = 0, \tag{6}$$

and therefore

$$\nabla p \cdot \mathbf{n} = 0. \tag{7}$$

The influence of the liner can be represented by specifying an appropriate surface impedance. The boundary condition at a compliant wall where the lining is locally reacting has been derived by Ingard [7]. He has shown that a proper formulation is based on the requirement of continuity of normal displacement, $\xi(x, t)$. For a wall which is parallel to the x co-ordinate, a natural boundary condition can be derived as follows.

The normal component of velocity at the wall can be expressed in terms of the convective derivative of the normal displacement

$$\mathbf{v} \cdot \mathbf{n} = \frac{\partial \xi}{\partial t} + U\frac{\partial \xi}{\partial x} \tag{8}$$

and pressure can be expressed in terms of impedance as

$$p = Z\frac{\partial \xi}{\partial t}. \tag{9}$$

The momentum equation in the radial direction is

$$\frac{\partial}{\partial t}(\mathbf{v} \cdot \mathbf{n}) + U\frac{\partial}{\partial x}(\mathbf{v} \cdot \mathbf{n}) = -\frac{1}{\rho_0}\frac{\partial p}{\partial n}. \tag{10}$$

For harmonic excitations of the form $\mathrm{e}^{\mathrm{i}\omega t}$, equations (8)–(10) can be written as

$$\mathbf{v} \cdot \mathbf{n} = \mathrm{i}\omega\left(1 - \mathrm{i}\frac{M}{k}\frac{\partial}{\partial x}\right)\xi, \qquad p = \mathrm{i}\omega Z\xi, \tag{11, 12}$$

$$\partial p/\partial \mathbf{n} = -\rho_0 \mathrm{i}\omega\left(1 - \mathrm{i}\frac{M}{k}\frac{\partial}{\partial x}\right)\mathbf{v} \cdot \mathbf{n}. \tag{13}$$

The boundary condition for a compliant surface thus emerges as

$$\frac{\partial p}{\partial r} = -\frac{\mathrm{i}k\rho_0 c}{Z}\left(1 - \mathrm{i}\frac{M}{k}\frac{\partial}{\partial x}\right)^2 p. \tag{14}$$

2.3. MODAL INTERFACE

As illustrated in Figure 2, the cylindrical computational domain is bounded on both ends by circular cross-sections. Since the computational domain is to be treated as a finite length of an infinite duct, there must be no reflections at these boundaries. Moreover, since a modal description of a duct pressure field is desirable, the pressure field at these boundaries should be expressed in terms of a weighted modal summation. At the hard-walled modal input plane, the modal expression must allow for both incident and reflected modes, with amplitudes and phases of the incident modes specified as an input. The pressure distribution at this cross-section is therefore expressed in terms of M incident and M reflected modes [8],

$$p = \sum_{j=0}^{M} (A_j^+ E_j + A_j^- E_j), \tag{15}$$

while at the hard-walled modal output plane

$$p = \sum_{j=0}^{M} (T_j E_j). \tag{16}$$

Here, E_j are the hard-walled cross-sectional modes. A_j^+ and A_j^-, which are complex numbers, are respective modal amplitudes of the right- and left-travelling modes at the modal input plane, while T_j are the modal amplitudes of the right-travelling modes at the modal exit plane. For a circular modal input plane, these modes can be expressed in terms of Bessel functions [9]:

$$E_{m,n}(r, \theta) = \mathrm{J}(k_{r,mn} r)\mathrm{e}^{-\mathrm{i}m\theta}. \tag{17}$$

Here n indicates the nth solution of the hard-walled boundary condition at the duct wall:

$$\mathrm{J}'_m(k_{r,mn} a) = 0. \tag{18}$$

This equation has an infinite number of solutions corresponding to $k_{r,mn}$, where the nth solution specifies the radial mode number for values in the range $n = [0, \infty]$. The sequence of $k_{r,mn}$ values signifies the set of radial modes, where $k_{r,mn}$ is the nth radial wavenumber and $k_{x,mn}$ is the corresponding axial wavenumber:

$$k_{r,mn}^2 = k^2 + k_{x,mn}^2(1 - M^2) - 2k_{x,mn}kM. \tag{19}$$

The integer m corresponds to the angular mode number, which can be positive or negative. Negative angular mode numbers correspond to clockwise spinning

modes, and a positive m indicates a counter-clockwise spinning mode. It is necessary to include both clockwise and counter-clockwise modes in the analysis since the asymmetry of the liner will excite modes in both circumferential directions. The M modes selected for an analysis should consist of all angular and radial modes which are cut-on, and an additional few above cut-off. Therefore, if the circumferential modal order ranges from $-\hat{m}$ to $+\hat{m}$ and the radial order varies from 0 to a maximum of $\hat{n}$, the total number of modes specified in the analysis is

$$M = (2\hat{m} + 1) \times \hat{n}. \tag{20}$$

The incoming modal amplitude is known *a priori*, but the amplitudes and phases of the reflected modes must be determined as part of the solution. The axial derivative, which will be used in the finite element derivation, can be expressed as

$$\frac{\partial p}{\partial x} = \sum_{j=0}^{M} (-\mathrm{i}k_{xj}^{+} A_j^{+} E_j - \mathrm{i}k_{xj}^{-} A_j^{-} E_j). \tag{21}$$

3. FINITE ELEMENT FORMULATION

3.1. EQUATIONS

Using a standard finite element Galerkin weighted residual procedure for equation (5) yields

$$\iiint_V \left\{ \nabla^2 p - M^2 \frac{\partial^2 p}{\partial x^2} \right\} W_i \, \mathrm{d}V + \iiint_V \left\{ k^2 p - 2\mathrm{i}kM \frac{\partial p}{\partial x} \right\} W_i \, \mathrm{d}V = 0. \tag{22}$$

Upon application of the divergence theorem to the second order spatial derivative terms in equation (22), an expression involving integrals over the computational domain volume and its surface emerges:

$$\iiint_V \left\{ k^2 p - 2\mathrm{i}kM \frac{\partial p}{\partial x} \right\} W_i \, \mathrm{d}V - \iiint_V \nabla W_i \cdot \left(\nabla p - \mathbf{i} M^2 \frac{\partial p}{\partial x} \right) \mathrm{d}V$$

$$+ \iint_S W_i \left(\nabla p - \mathbf{i} M^2 \frac{\partial p}{\partial x} \right) \cdot \mathbf{n} \, \mathrm{d}S = 0. \tag{23}$$

As with the previous surface integral expressions, the normal gradient of the solution variable, the complex acoustic pressure (p), is used to implement the aeroacoustic natural boundary conditions. The term $\mathbf{i} \cdot \mathbf{n}$ is zero on solid boundaries, since in the domain treated here all solid surfaces in the computational domain are aligned with the direction of uniform flow.

3.2. BOUNDARY CONDITIONS

For the case of a compliant wall [10], the boundary term is derived by using equation (14), which yields

$$-\mathrm{i}kc\rho_0 \int_S AW_i\left(1 - \frac{M^2}{k^2}\frac{\partial^2}{\partial x^2} - 2\mathrm{i}\frac{M}{k}\frac{\partial}{\partial x}\right)p \,\mathrm{d}S, \tag{24}$$

where A, the reciprocal of the specific acoustic impedance, is the admittance. Upon integrating the second order terms by parts this boundary integral term reduces to

$$-\mathrm{i}k\rho_0 c \int_S AW_i p \,\mathrm{d}S - 2M\rho_0 c \int_S AW_i \frac{\partial p}{\partial x}\,\mathrm{d}S$$

$$-\mathrm{i}\,\frac{M^2\rho_0 c}{k}\int_S A\,\frac{\partial W_i}{\partial x}\frac{\partial p}{\partial x}\,\mathrm{d}S + \mathrm{i}\,\frac{M^2\rho_0 c}{k}\oint_C AW_i\frac{\partial p}{\partial x}n_x\,\mathrm{d}C. \tag{25}$$

3.3. MODAL INTERFACE

At the modal input plane, the modal expression for pressure (equation (15)) and for its axial derivative (equation (21)) can be incorporated into the finite element formulation through the surface integral boundary condition [8]:

$$-\int_S W_i(1 - M^2)\frac{\partial p}{\partial x}\,\mathrm{d}S. \tag{26}$$

The negative sign indicates that the condition is directed into the surface, in the opposite direction to the outward normal. The finite element equation can now be expressed as

$$[K]\{\phi\} + [B^-]\{A^-\} = -[B^+]\{A^+\}, \tag{27}$$

where

$$B_{ij}^{\pm} = (1 - M^2)\,\mathrm{i}\int_S W_i k_{x_j}^{\pm} E_j \,\mathrm{d}S. \tag{28}$$

This equation set may now be under-determined because of the extra solution unknowns—the reflected modal amplitudes. Equation (15) is used to yield the necessary additional equation. Using a weighting function

$$W_i = \mathrm{i}(1 - M^2)k_{x_i}^{-}E_i^*, \tag{29}$$

where E^* is the complex conjugate of E,

$$E_{m,n}^*(r, \theta) = \mathrm{J}_m(k_{r,mn}r)\,\mathrm{e}^{\mathrm{i}m\theta}, \tag{30}$$

and integrating over the duct cross-section where the boundary condition is applied gives

$$\int_S pW_i \, \mathrm{d}S = \int_S \mathrm{i}(1 - M^2) k_{x_i}^- E_i^* E_j \, \mathrm{d}S A_j^+ + \int_S \mathrm{i}(1 - M^2) k_{x_i}^- E_i^* E_j \, \mathrm{d}S A_j^- . \quad (31)$$

Following from previous axisymmetric work [8], it would appear logical to use E in the weighting function (equation (29)). This is not appropriate for the three-dimensional application, however, because the integral of the product $E_i E_j$ over a circular surface can be zero, which results in zero terms on the diagonal of the system matrix as follows:

$$\int_S E_{m,n}(r, \theta) E_{m,n}(r, \theta) \, \mathrm{d}r \, \mathrm{d}\theta = \int_0^{2\pi} \int_0^a \mathrm{J}_m^2(k_{r,mn} r) \, \mathrm{e}^{\mathrm{i}(-2m)\theta} \, \mathrm{d}r \, \mathrm{d}\theta = 0, \quad m \neq 0. \quad (32)$$

Using E^* results in diagonal terms of the form

$$\int_S E_{m,n}^*(r, \theta) E_{m,n}(r,\theta) \, \mathrm{d}r \, \mathrm{d}\theta = \int_0^{2\pi} \int_0^a \mathrm{J}_m^2(k_{r,mn} r) \, \mathrm{d}r \, \mathrm{d}\theta, \quad (33)$$

where it can be seen that the exponential in θ has been eliminated.

Equation (31) can be expressed as

$$[C]\{p\} + [D]\{A^-\} = -[D]\{A^+\}, \quad (34)$$

where

$$D_{ij} = -\mathrm{i}(1 - M^2) \int_S k_{x_i}^- E_i^* E_j \, \mathrm{d}S \quad \text{and} \quad C_{ij} = \mathrm{i}(1 - M^2) \int_S k_{x_i}^- E_i^* N_j \, \mathrm{d}S. \quad (35, 36)$$

For a hard-walled duct section, the modes are orthogonal so that only D_{ii} terms are non-zero, which results in a diagonal matrix.

The complete coupled system of equations can be expressed as

$$\begin{bmatrix} [K]_{N \times N} & [B^-]_{N \times M} \\ [C]_{M \times N} & [D]_{M \times M} \end{bmatrix} \begin{bmatrix} \{p\}_{N \times 1} \\ \{A^-\}_{M \times 1} \end{bmatrix} = - \begin{bmatrix} [B^+]_{N \times M} \\ [D]_{M \times M} \end{bmatrix} \{A^+\}_{M \times 1}. \quad (37)$$

The size and form of the matrices is indicated here by the integer products. M is the number of modes allocated for the analysis and N is the number of nodes in the finite element model.

A second coupling procedure is used on the hard-walled modal exit plane. In this case, however, only the transmitted modal amplitudes, T, arise in the finite

element expression. The overall equation system, with modal coupling terms for the incident, reflected and transmitted modes is

$$\begin{bmatrix} [K]_{N\times N} & [B^-]_{N\times M} & [B_2^-]_{N\times M} \\ [C]_{M\times N} & [D]_{M\times M} & [0]_{M\times M} \\ [C_2]_{M\times N} & [0]_{M\times M} & [D_2]_{M\times M} \end{bmatrix} \begin{bmatrix} \{p\}_{N\times 1} \\ \{A^-\}_{M\times 1} \\ [T]_{M\times N} \end{bmatrix} = - \begin{bmatrix} [B^+]_{N\times M} \\ [D]_{M\times M} \\ [0]_{M\times M} \end{bmatrix} \{A^+\}_{M\times 1}, \tag{38}$$

where the subscript 2 indicates coupling matrices evaluated at the modal exit plane. Here M is the total number of modes specified at both the inlet and outlet plane.

Since all possible modes can be accounted for by using this modal coupling procedure, the modal boundaries can theoretically be specified at any hard-walled section in the infinite duct. In practice, the number of modes is limited by including all cut-on modes plus an additional few above cut-off and positioning the modal boundary sufficiently distant from any duct non-uniformities so that the cut-off modes have largely decayed.

4. SOLUTION PROCEDURE

The duct acoustic problems under consideration here can yield large systems of equations for higher frequencies. The domain is three-dimensional and a certain mesh density, typically at least five quadratic elements per wavelength, must be maintained in each co-ordinate direction if acceptable solutions are to be obtained [4, 5]. In this paper, 20 node hexahedral, serendipity, reduced integration elements have been employed in all cases, with a minimum mesh density of five elements per wavelength.

Traditionally, finite element schemes have used a variety of direct solution methods. All direct solvers, however, generate fill-in terms as the solution proceeds, so that the storage requirement is greatly increased over the size of the original sparse system matrix. As a result, direct solution schemes cannot effectively be used to solve for large systems because the storage demands become prohibitively large. As an alternative, we avail ourselves of iterative solution techniques to solve the finite element acoustic problems [4, 5]. Iterative solvers are attractive because they only involve operations on the original system matrix, so that throughout the solution procedure the storage requirement is restricted to the non-zero matrix terms. To take full advantage of these storage savings, it is necessary to implement a sparse storage scheme which only stores and operates on these non-zero terms.

The primary weakness of applying iterative solvers to the current acoustic problems is their lack of robustness. This difficulty is addressed by implementing a preconditioner [11]. In this work we use a preconditioner based on incomplete lower and upper triangular (ILU) decomposition. This is a two-parameter $ILUT(p, t)$ system [11] which allows the strength and associated cost of the preconditioner to be adjusted for systems of varying difficulty. The first parameter (p) limits the number of terms to be generated per row of the preconditioner matrix, and the second (t) is a magnitude tolerance which determines which fill-in

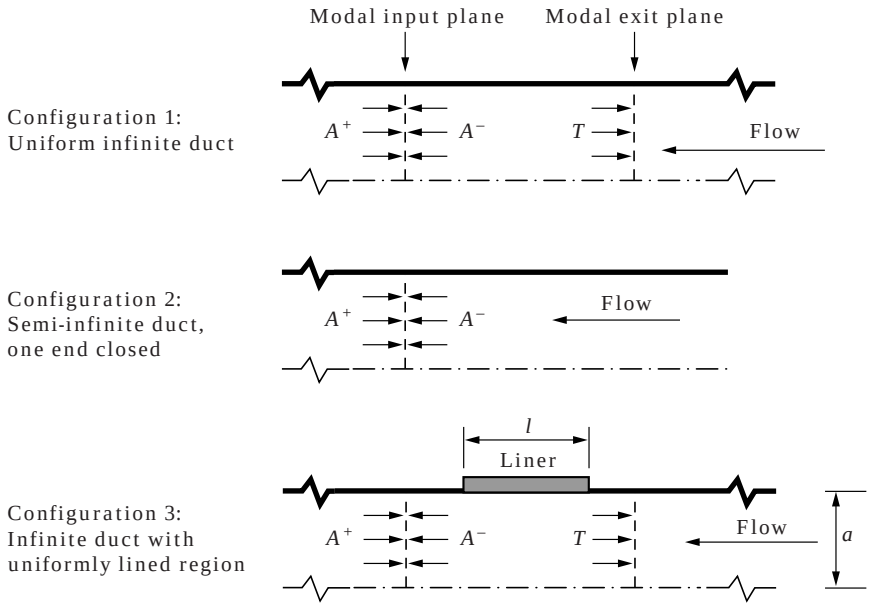

Figure 3. Circular duct configurations used for verification.

terms are to be dropped. To maximize computational efficiency, this procedure is applied in conjuction with a sparse storage and operation routine.

Having conducted extensive studies [4, 5] to determine the optimal combination of iterative solver and preconditioner for solving the Helmholtz equation, we found that the biconjugate gradient [12] method combined with a basic $ILU(0)$ preconditioner, where the L and U matrices assume the same structure as K, generally ensures reasonable convergence for the three-dimensional duct acoustic problems under consideration here.

5. VERIFICATION

Extensive verification studies [4, 5] have already been performed on the current finite element method by comparing predictions with known analytical solutions. In these tests the effect of mesh density on pressure amplitude and phase was determined. To verify the new double modal coupling condition and the compliant wall boundary condition, a series of simple duct test cases are now examined. Three fundamental cylindrical duct test configurations, as illustrated in Figure 3, are used for this verification. Configuration 1 consist of an infinite hard-walled duct with uniform flow; Configuration 2 is a semi-infinite hard-walled duct with uniform flow and one end closed by an acoustically hard-walled termination; Configuration 3 is an infinite duct with uniform flow and a finite uniformly lined region. We note here that because we have specified a negative reactance in some of the verification configurations, unstable surface modes [13, 14] can theoretically arise. For most practical applications, however, these surface modes are generally of minor importance [14].

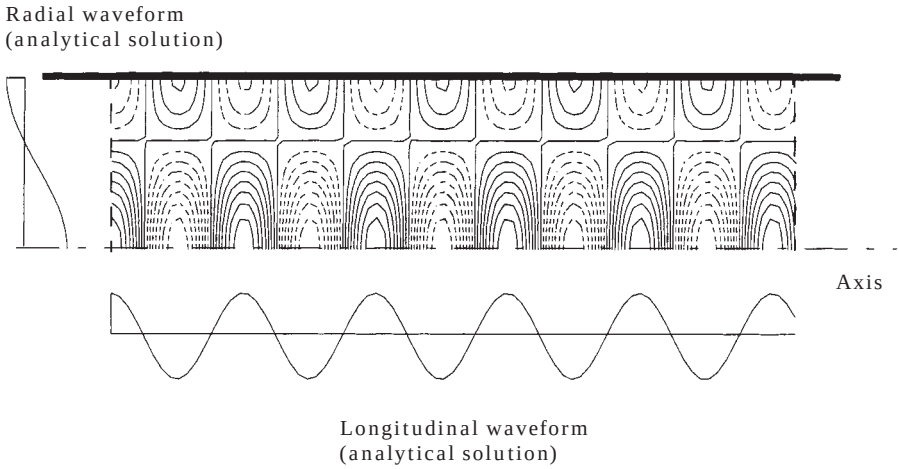

Figure 4. Numerical prediction of real pressure contours for mode (0, 1) in Configuration 1 and corresponding exact waveform solutions, $M = -0{\cdot}5$, $ka = 5{\cdot}0$.

5.1. CONFIGURATIONS 1 AND 2: HARD WALL CASES

Configuration 1 is used to verify the predictions for the case of an incident mode at the modal input plane and its transmission at the modal exit plane. All cut-on modes, plus a few above cut-off, are included in the modal coupling procedure, and a cut-on modal amplitude and phase are specified at the modal input plane. At the modal exit plane, the modal amplitude ought to be unchanged, and the phase shift should be as indicated by the analytical solution. All other modal transmisson amplitudes should be zero. The numerical model was verified for this configuration for a large variety of modes, over a range of different frequencies and Mach numbers. An example is illustrated in Figure 4 for a length of an infinite

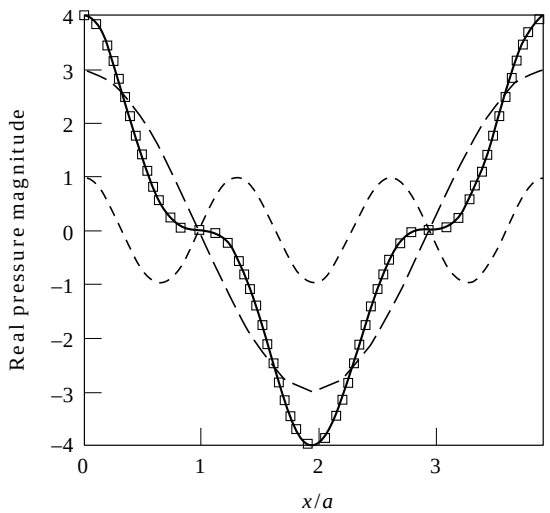

Figure 5. Comparison of numerical predictions and semi-analytical solutions of real pressure distribution for mode (0, 0) in Configuration 2; $M = -0{\cdot}5$, $ka = 2{\cdot}41$. – – –, Incident wave; ----, reflected wave; ——, semi-analytical solution; □, finite element solution.

TABLE 1

Configuration 3: *parameter sets used in compliant wall test cases*

Case	$Z/\rho_0 c$	Mach No.	Mode	ka
1	(1, −2)	0·0	(0, 0)	1·5
2	(1, −2)	−0·3	(0, 0)	1·5
3	(2, −1)	−0·3	(0, 2)	7·4
4	(3, 0)	−0·3	(5, 0)	7·4

cylindrical duct, where the finite element prediction of real pressure contours and corresponding analytical waveforms for mode (0, 1) are shown.

Although a uniform flow field in a closed duct is physically unrealistic, it provides a useful test case for verification purposes. The semi-infinite, closed duct of Configuration 2 is used to verify the correct prediction of reflected modal amplitudes at the modal input plane. Specifying the amplitude of one incident cut-on mode should result in a reflected modal amplitude of the same magnitude, with an appropriate phase shift. Again, this test was performed for many different modes over a range of frequencies and Mach numbers. A typical result for this configuration is shown in Figure 5, where finite element and analytical solutions of real pressure distributions for mode (0, 0) are compared. Analytically, for this test case the ratio of incident to reflected modal amplitudes is

$$A^-/A^+ = \sqrt{(1-M)^2/(1+M)^2} = 3. \tag{39}$$

To five decimal places, the predicted reflected modal amplitude was 3·0 for the plane wave and 0·0 for all others.

5.2. CONFIGURATION 3: COMPLIANT WALL

Configuration 3 is an appropriate test case, since from a numerical point of view the longitudinal step change in impedance in this arrangement is analogous to a circumferential step change. If the three-dimensional finite element method can correctly model the effect of the axial variation, it is a good indication that it should also be able to treat the circumferential variation present in a spliced liner. In addition to proving the modal coupling scheme at both the modal input and exit planes, this configuration also tests the impedance boundary condition.

To validate the finite model for this compliant wall arrangement, predictions for four test cases based on Configuration 3 (see Table 1) are compared with solutions from a semi-analytical code [15] which was developed at the National Aerospace Laboratory (NLR), The Netherlands. The NLR method is an extension of techniques developed by Rienstra [13, 16]. Modes are input at one end of the duct, where a modal amplitude distribution is specified; the boundary at the input end is assumed transparent to reflected modes, and the other end of the duct is also anechoic. The computational domain, representing a finite length of the infinite duct, consists of a cylinder of length 1·0 m and radius 0·2 m, with a region of the duct wall, between $x = 0{\cdot}3$ and $x = 0{\cdot}7$, which is compliant. To model the

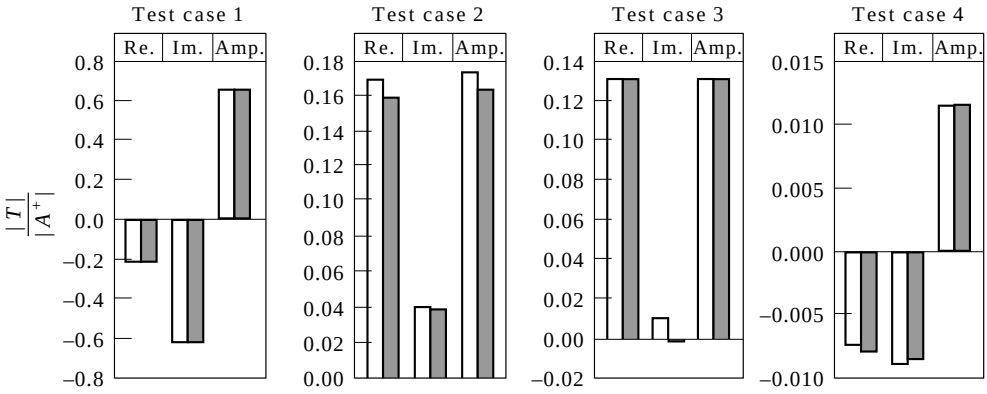

Figure 6. Comparison of numerical predictions and semi-analytical solutions of transmitted modal amplitudes for Configuration 3 for different input modes. □, finite element; ■, semi-analytical.

compliant wall, an appropriate impedance is specified, as shown in Table 1. Solutions are predicted at reduced frequencies of $ka = 1{\cdot}5$ and $ka = 7{\cdot}4$.

Computed values for the transmitted, normalized modal amplitudes of the energized mode in each test case are compared in Figure 6. It can be seen that there is close agreement between the numerical and semi-analytical predictions. In Figure 7, field results are plotted as contours of the amplitude of the computed complex pressure, P. Again, there is close agreement between the finite element and semi-analytical predictions. For direct comparison purposes the contours

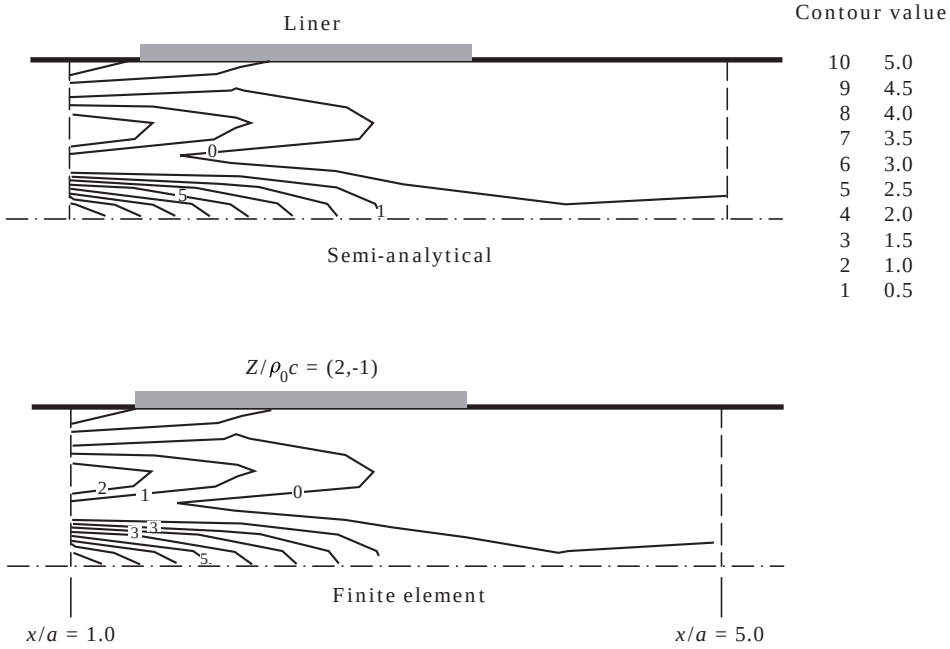

Figure 7. Comparison of numerical predictions and semi-analytical solutions of duct pressure amplitude contours for Configuration 3. $M = -0{\cdot}3$, $ka = 7{\cdot}4$, mode (0, 2), $l/a = 0{\cdot}4$.

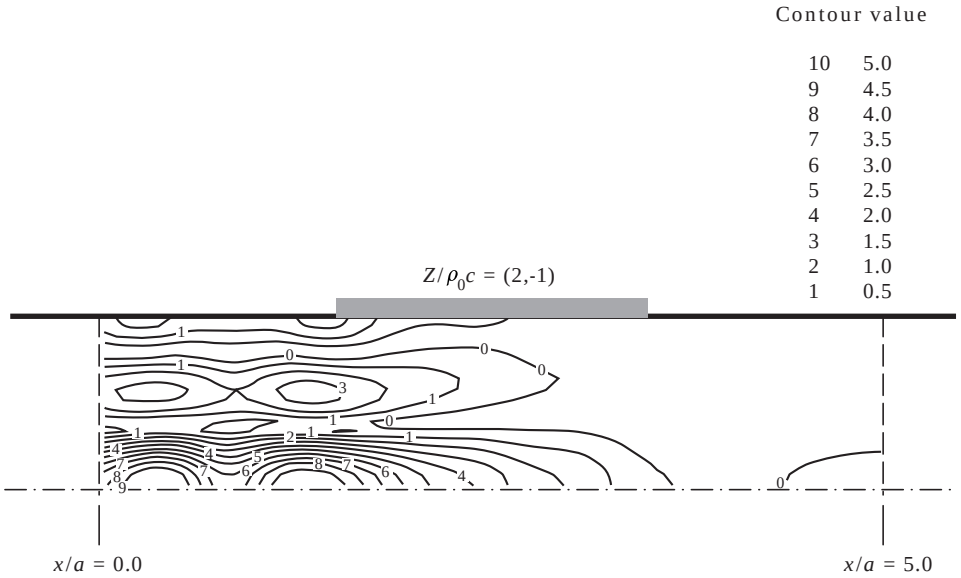

Figure 8. Numerical solution of duct pressure (plotted using all nodal points) for Configuration 3. Parameter values as Figure 7.

plotted in Figures 7(a) and (b) were bi-linearly interpolated from discrete values on a coarse grid ($x/a = 1, 2, 3, 4, 5$ and $r/a = 0{\cdot}0, 0{\cdot}1, \ldots, 0{\cdot}9, 1{\cdot}0$). Apart from giving a jagged appearance to the contours, the pattern is misleading, as shown in Figure 8, where the "true" finite element solution is replotted using all the nodal points employed in the solution process.

It is encouraging that the finite element semi-analytical solutions agree closely for the case of a liner with a longitudinal step change in impedance. In light of

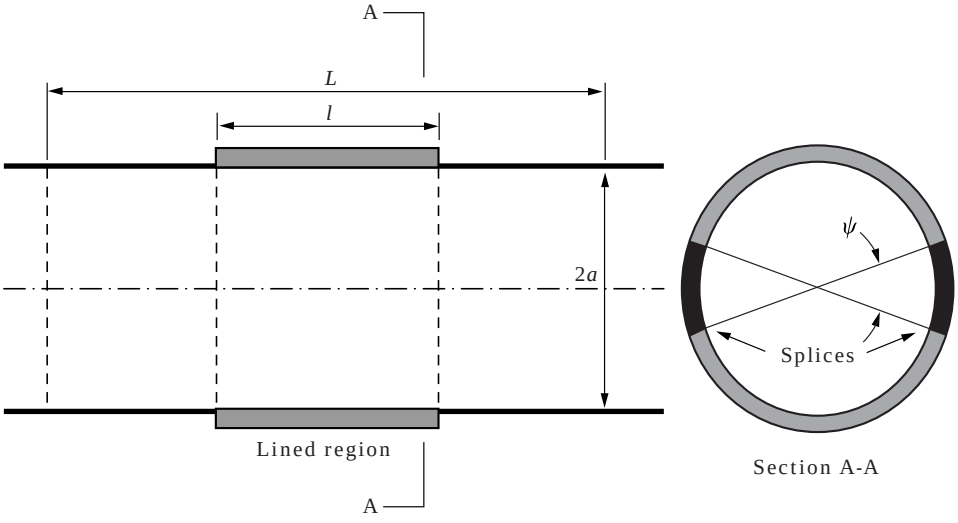

Figure 9. Configuration 4 and 5: test for infinite duct with region of longitudinally-spliced liner. For Configuration 4, $\psi = 0{\cdot}75$, $l/a = 2$, $L/a = 5$; for configuration 5 $\psi = 0{\cdot}15$, $l/a = 0{\cdot}6$, $L/a = 1{\cdot}5$.

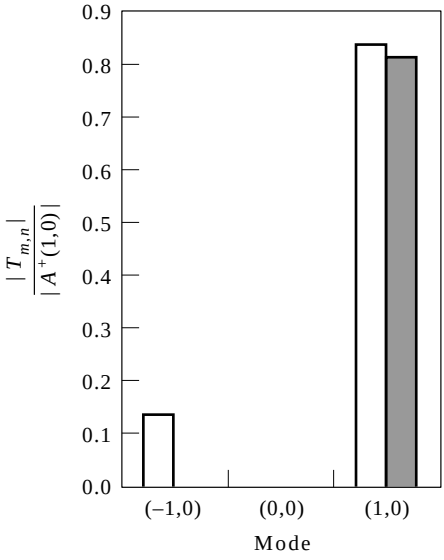

Figure 10. Comparison of numerical predictions of transmitted modal amplitudes for uniform liner and for two-splice liner at $ka = 2{\cdot}2$ (Configurations 3 and 4). ■, Uniform liner (Configuration 3); □, spliced liner (Configuration 4).

these test results, we now proceed to investigate the effect of longitudinal splices in a lined duct.

6. APPLICATION

6.1. CONFIGURATION 4

The method is now applied to a duct with a two-splice liner. Liner Configuration 4, which contains two hard-walled splices, is illustrated in Figure 9. The splices are diametrically opposed and each extends circumferentially over an angle of 0·75 rad. The lined region of the infinite duct is 0·4 m long, and is located at the centre of the test domain, which consists of a cylinder, 1 m long, 0·4 m diameter. For a Mach number of zero, the non-dimensional impedance of the liner is specified as follows: a resistance of 1·5, a mass reactance of $0{\cdot}01k$ and a cavity reactance of $-\cot(0{\cdot}016k)$. Thus

$$Z/\rho_0 c = 1{\cdot}5 + \mathrm{i}(0{\cdot}01k - \cot(0{\cdot}016k)). \tag{40}$$

To investigate the effect of the liner splices, a single incident mode is injected and the resulting transmitted modal spectrum is calculated. These spectra are compared with the transmitted field produced by a uniform homogeneous liner modelled under the same conditions (Configuration 3). In ever case, all transmitted modal amplitudes are normalized with respect to the amplitude of the single energized incident mode.

The first set of calculations are performed at 600 Hz, which corresponds to a ka value of 2·2. At this frequency, only modes $(-1, 0)$, $(0, 0)$ and $(1, 0)$ are cut-on, so that the effect of the scattering on a single incident mode should be easy to

isolate. Exciting the incident mode (1, 0) and solving for both the uniform and spliced configurations yields the transmitted spectra which are compared in Figure 10. The transmitted amplitude for the spliced arrangement is larger than for the uniform liner, which is to be expected, since the latter has a greater lined surface area. Also, scattering effects cause mode $(-1, 0)$ to be excited and transmitted. By analogy with rotor–stator interaction theory [17], the circumferential order of the modes which are excited by the scattering can be specified by the sequence

$$m = m_I \pm lN_S. \tag{41}$$

Here m_I is the circumferential order of the excited incident mode, l is an arbitrary integer, and N_S is the number of splices. Thus, if mode (1, 0) is excited as an incident mode, and a liner with two splices is used, modes of circumferential order -1 and 1 will also be excited, as correctly predicted by the numerical method for this test case.

As a check on the influence of the incident mode phase on the transmitted spectrum, the tests were re-run for a range of different phases. No noticeable difference in the transmitted amplitudes was observed.

A second test was conducted at 1830 Hz, corresponding to a wavenumber $ka = 6{\cdot}8$. This frequency was chosen to demonstrate the behaviour described by equation (41) over a broader range of circumferential modal orders. In this case, all zero-order radial modes of circumferential order less than six are cut-on, in addition to first-order radial modes of circumferential order less than three. In Figure 11, it can be seen that only modes of first circumferential order are transmitted when a uniform liner is used. This behaviour is to be expected, since for an axisymmetric duct there is no mechanism to generate modes of other circumferential orders. However, as evident in Figure 12, a spliced liner scatters

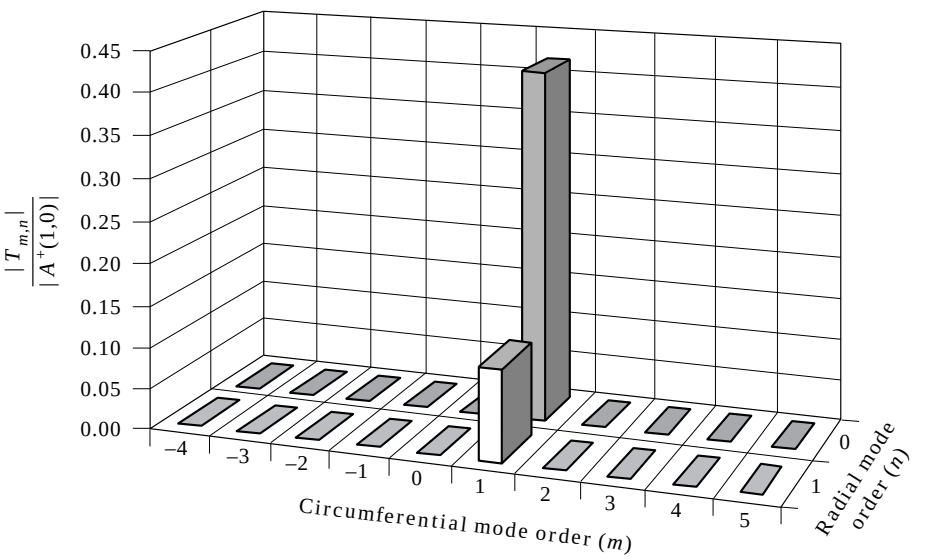

Figure 11. Numerical prediction of transmitted modal amplitudes for uniform liner and incident mode (1, 0) at $ka = 6{\cdot}8$; Configuration 3.

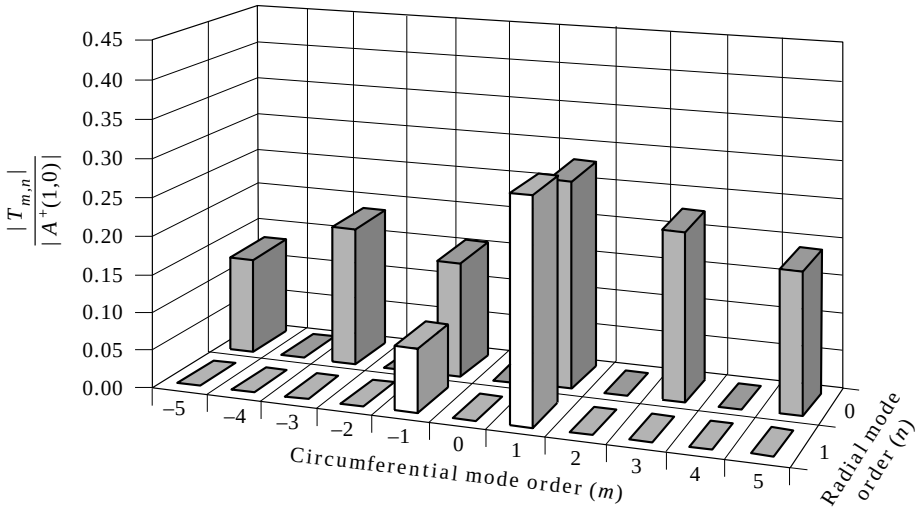

Figure 12. Numerical predication of transmitted modal amplitudes for two-splice liner ($\psi = 0{\cdot}75$) and incident mode (1, 0) at $ka = 6{\cdot}8$; Configuration 4.

the incident mode, causing modes of several circumferential orders to be excited. It can be seen that the excited modes follow the periodic pattern governed by equation (41). Only cut-on modes of circumferential order $-5, -3, -1, +1, +3, +5$ are observed in the transmitted spectrum.

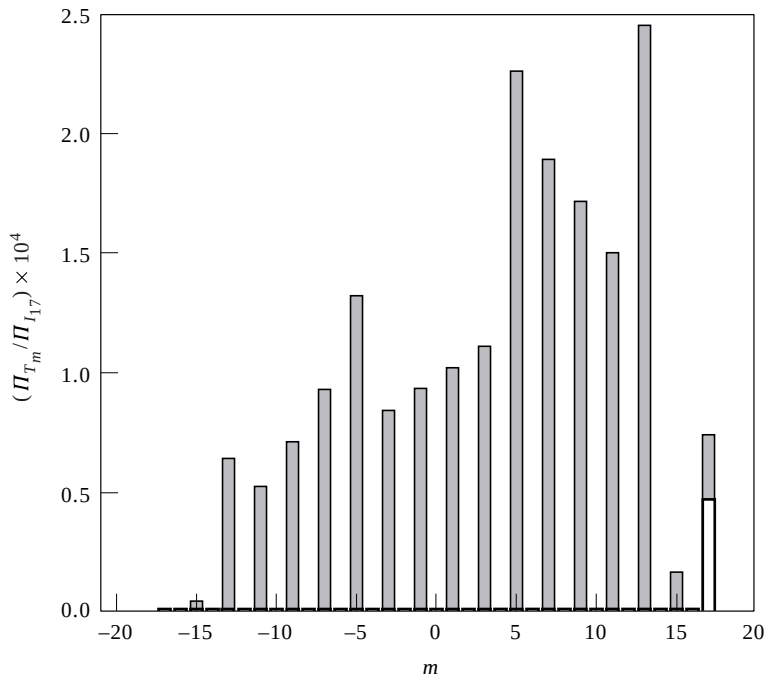

Figure 13. Numerical prediction of transmitted modal amplitudes for two-splice liner ($\psi = 0{\cdot}15$) and incident mode (17, 0) at $ka = 20{\cdot}0$; Configuration 5. ■, Two-splice liner; □, uniform liner.

6.2. CONFIGURATION 5

In a real turbofan engine inlet, splices are narrower and frequencies are considerably higher than those just considered. To demonstrate the ability of the numerical method to treat a realistic configuration, a periodic two-splice liner ($Z/\rho_0 c = (2, -1)$, $\psi = 0{\cdot}15$, $l/D = 0{\cdot}3$) is analyzed. For a single incident mode ($m = 17$, $n = 0$), the solutions are computed at $ka = 20{\cdot}0$ with $M = -0{\cdot}3$ for both the uniform and spliced liners. In Figure 13, the transmitted modal spectra are compared. Results are presented in terms of the transmitted acoustic power of each modal order, normalised with respect to the power of the single incident mode. For this frequency, modes of circumferential order greater than 18 are cut-off. As before, the presence of liner splices cause cut-on modal orders to be excited in the sequence described by equation (41) with the amplitudes of even order modes calculated as zero to a precision of seven significant figures. The splices result in the transfer of energy to lower order modes which are less well attenuated, and because of this, the insertion loss for the spliced liner is far smaller than that of the uniform equivalent. Indeed, 40 times (16 dB) more power is transmitted by the spliced liner. However, for these conditions, both the uniform and spliced liners have relatively large insertion losses (27·0 and 43·0 dB respectively) because mode (17, 0) is close to cut-off and thus well attenuated. Overall, the influence of the splices is not particularly important, and the power transfer due to scattering by the splices is seen to be negliglible, with ($\Pi_{T_m}/\Pi_{I_{17}} < 10^{-3}$).

These test cases have demonstrated the usefulness of this numerical approach in analyzing the scattering effect of splices in a liner. Moreover, it is encouraging that the numerical predictions show expected trends and characteristics. On the bases of these results, it is clear that liner splices can significantly influence the transmitted acoustic field and the need for further investigation is evident. Since the method is fully three-dimensional, it is applicable also to non-circular ducts and to liner layouts of arbitrary shape and impedance property distributions. A logical next stage would be to study and to quantify the effect of splice configuration on the transmitted spectrum, examining aspects such as splice number, spacing, width and shape. Such a study may well indicate how best to reduce any adverse scattering effects

7. CONCLUSIONS

In this paper we have described the development of a three-dimensional finite element technique which can model the effect of longitudinal linear splices on the transmitted acoustic field in a duct. The theoretical model considered here consists of a length of liner installed in an infinite cylindrical duct with a uniform, unidirectional flow. The liner is represented by an impedance boundary condition, and since the method enables arbitrary surface impedance distributions to be treated, a liner consisting of several segments divided by hard-walled intercostal strips is investigated. By expressing the cross-sectional pressure distribution as a weighted summation of duct modes, modal coupling conditions are implemented at both ends of the computational domain to enfore anechoic radiation conditions. With this technique, incident modes of a specified amplitude and phase are injected

at one end of the domain and the transmitted amplitudes and phases are predicted at the other boundary.

The technique was verified by using a series of fundamental duct configurations. To compare predictions with known analytical solutions, simple hard-walled configurations were used to test the modal coupling schemes. For the case of a cylindrical duct with a uniform axisymmetric length of liner, numerical predictions were compared with solutions from a semi-analytical method. Since, from a numerical perspective, a longitudinal step change in impedance is analogous to a circumferential step change, this test is a good indication of the ability of the method to model a spliced liner. To demonstrate the potential and usefulness of this simulation procedure, we compared predictions for the transmitted modal spectra of a duct containing a uniform liner with that of a duct containing a two-splice liner. The scattering effect of the splices was clearly demonstrated in the transmitted modal spectrum with the appearance of circumferential modes of orders different from that of the excitation mode. An expresssion relating the circumferential order of excited modes to the incident modal order and the number of splices was presented, and it was shown that the transmitted modal spectra in all test cases was governed by this equation. Interestingly, when realistically sized splices were considered at $ka = 20$, the overall effect of liner non-uniformities on the transmitted power was insignificant for the incident mode (17, 0). Nevertheless, these results demonstrate the potential influence of liner non-uniformities on transmitted modes and indicate the need for further investigation.

ACKNOWLEDGMENTS

The authors would like to thank Pieter Sijtsma, (National Aerospace Laboratory, The Netherlands), for providing the semi-analytical duct solutions for Configuration 3.

REFERENCES

1. S. L. Sarin and E. R. Rademaker 1993 *AIAA Paper* 93–4414, In flight acoustic mode measurements in the turbofan engine inlet of Fokker 100 aircraft.
2. D. G. Henshaw 1996 FANPAC-RR-96-9.1, *Rolls Royce*, *Derby*, *August* 1996. Aeroacoustics methods for fan noise prediction and control; FAN-PAC Final Technical Report.
3. E. R. Rademaker, S. L. Sarin and C. A. Parente 1996 *AIAA Paper* 96–1682. Experimental investigation on the influence of liner non-uniformities on prevailing modes.
4. B. A. Regan and J. A. Eaton 1995 *CEAS/AIAA Paper* 95–012. Application of an efficient iterative 3D finite element scheme to the fan noise radiation problem.
5. B. A. Regan 1996 *Ph.D. Dissertation*, *National University of Ireland*, *Galway*, *Ireland*. Development of finite element techniques for aeroacoustic applications.
6. B. A. Regan and J. A. Eaton Modelling of aeroacoustic field radiation for turbofan nacelles with scarfed inlet geometries.
7. U. Ingard 1959 *Journal of the Acoustical Society of America* **29**, 435–441. Influence of fluid motion past a plane boundary on sound reflection, absorption and transmission.

8. R. J. Astley and W. Eversman 1983 *AIAA Paper* 83–0709. Wave envelope and infinite element schemes for fan noise radiation from turbofan inlets.
9. M. L. Munjal 1987 *Acoustics of Ducts and Mufflers*, New York: Wiley.
10. K. J. Baumeister and W. Eversman 1988 *Journal of Propulsion* **5**(1). Effects of wind-tunnel wall absorption on acoustic radiation of propellers.
11. Y. Saad 1988 *Journal of Computational and Applied Mathematics* **24**, 89–105. Preconditioning techniques for nonsymmetric and indefinite linear systems.
12. H. A. Van der Vorst 1992 *SIAM Journal of Scientific and Statistical Computing* **13**, 631–644. Bi-CGSTAB: a fast and smoothly converging variant of Bi-CG for the solution of nonsymmetric linear systems.
13. S. W. Rienstra 1986 *Proceedings of Ne*, *IUTAM symposium*, *Lyon* (editors G. Comte-Bellot and J. E. Ffowes Williams). Hydraulic instabilities and surface waves in a flow over an impedance wall, aero- and hydro-acoustics.
14. W. Koch and W. Mohring 1983 *AIAA Journal* **21**(2), 200–213. Eigensolutions for liners in uniform mean flow ducts.
15. E. R. Rademaker 1990 *ASME Paper* 90-WA/NCA-2. Experimental validation of a lined duct acoustics model including flow.
16. S. W. Rienstra 1984 *Journal of Sound and Vibration* **94**(2), 267–288. Acoustic radiation from a semi-infinite annular duct in a uniform subsonic mean flow.
17. J. M. Tyler and T. G. Sofrin 1962 *SAE Transactions* **70**, 309–332. Axial flow compressor noise studies.

APPENDIX: NOMENCLATURE

A	acoustic admittance
A^+	complex amplitude of input mode
A^-	complex amplitude of reflected mode
a	duct radius
B_{ij}	finite element modal coupling matrix
C	boundary of surface S
C_{ij}	finite element modal coupling matrix
c	speed of sound
D_{ij}	finite element modal coupling matrix
E	duct cross-sectional mode
$\mathbf{i}$	unit normal vector in the x direction
i	$\sqrt{-1}$
J	Bessel function
K_{ij}	finite element system matrix
k	wavenumber
$k_x^{\pm}$	axial wavenumber in the $(+x)$ or $(-x)$ direction
k_r	radial wavenumber
l	length of lined region; arbitrary integer
L	lower decomposed component of matrix; length of duct computational domain
M	number of duct modes included in analysis; Mach number
m	circumferential modal order
$\hat{m}$	maximum circumferential modal order
m_I	circumferential order of the excited incident mode
N	number of nodes in finite element model
N_i, N_j	finite element shape functions
N_S	number of liner splices
n	radial modal order
$\hat{n}$	maximum radial modal order
$\mathbf{n}$	unit vector in the outward surface normal direction
n_x	direction cosine between surface normal and x direction

p acoustic pressure
S surface of computational volume
T amplitude of transmitted mode
U uniform steady flowfield velocity; upper decomposed form of matrix
$\mathbf{v}$ acoustic velocity vector
W finite element weighting function
Z specific acoustic impedance
ψ circumferential angle subtended by intercostal strip
ξ normal displacement of compliant surface
Π_{I_m} total incident modal power of all modes of circumferential order m
Π_{T_m} total transmitted modal power of all modes of circumferential order m
ρ_0 steady fluid density